ACS Photonics

pubs.acs.org/journal/apchd5

Letter

Coherent Multilayer Photonic Nanoantenna Array with off-Aperture Phase Adjustment

Farshid Ashtiani* and Firooz Aflatouni

Cite This: https://doi.org/10.1021/acsphotonics.1c00608

Read Online

ACCESS | Metrics & More | Article Recommendations | Supporting Information

ABSTRACT: Two-dimensional optical beam-steering with applications in LiDAR, projection, imaging, and communication is performed using either a 2-D optical phased array (OPA) with per-element optical phase control or a 1-D OPA with a combination of phase control and wavelength tuning. The former typically suffers from a high power consumption and a large element-spacing, and the latter requires a highly tunable laser and is incompatible with certain 2-D beam-steering applications such as communication. In either case, achieving subwavelength element-spacing is challenging due to the large size of devices compared to the operation wavelength. Here, we report a single-wavelength multilayer 2-D OPA, where a beam is formed through near-field interference of waves emitted from array elements on each layer. Vertically aligned tilted optical nanoantennas, 3-D optical signal distribution, and off-aperture phase control enable the realization of a record element-pitch of 3 μm. The 64-element 2-D OPA achieves a steering range of 23° using only 16 phase shifters.

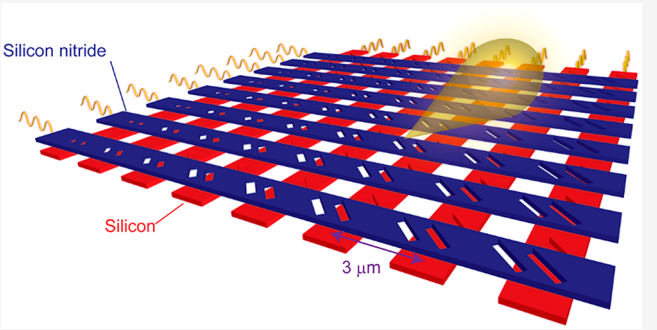

KEYWORDS: *photonic nanoantenna, optical phased array, multilayer photonics, silicon photonics, silicon nitride, grating structures*

An optical phased array (OPA) consists of a one- or two-dimensional array of optical antennas used to receive/transmit optical signals from/toward a specific spatial direction.[1−20] In many applications such as LiDAR systems, it is desired to utilize a large array aperture size and small element-spacing (ideally half of the wavelength) to form a narrow optical beam that is steerable over a wide range with a high side-lobs suppression. Two-dimensional optical beam-steering is typically performed using two main methods: either a 1-D array of grating-based optical antennas is used, where the formed beam is steered in one dimension by adjusting the relative phase between the antenna elements and in the other dimension through wavelength tuning,[11−20] or a 2-D phased array is used, where beam-steering in both dimensions is performed through relative phase adjustments between the antenna elements.[1−4,7−10] Despite excellent performance, the former requires a highly tunable laser source and is not compatible with some class of applications such as optical communication and the latter suffers from large element spacing due to the comparable size of the photonic devices with the wavelength of operation and also optical and electrical routing complexities, resulting in the presence of side lobes and a limited steering range.

Here we report the demonstration of a single wavelength 2-D compact OPA, where vertically aligned nanoantennas implemented on silicon (Si) and silicon nitride (SiN), 3-D light distribution and processing, and off-aperture relative phase adjustment between nanoantennas on each layer enable the realization of the smallest element pitch implemented for a 2-D OPA to date with significantly reduced per-element power consumption. A record element pitch of 3 μm is achieved for the implemented 8 × 8 OPA, while only 16 off-aperture phase shifters are used, reducing the per-element power consumption by a factor of 4. In general, our phased array architecture enables a power consumption reduction factor of $N/2$ for an $N \times N$ array.[21] The implemented OPA was used to demonstrate 2-D beam-steering over a range of about 23° without wavelength tuning, making the proposed OPA architecture compatible with many applications such as a free-space optical communicant, LiDAR, and 3-D imaging to name a few.

To implement the proposed OPA, a commercial silicon photonic process that features two layers of photonic devices in Si and SiN was used. Figure 1a shows the photonic layer-stack of the fabrication process used for the proposed OPA. In this figure, two single-mode nanophotonic waveguides on Si and SiN layers with 80 nm vertical spacing are shown. In addition, the fundamental optical modes in each waveguide when separately excited at 1550 nm are illustrated. All on-chip

Received: April 21, 2021

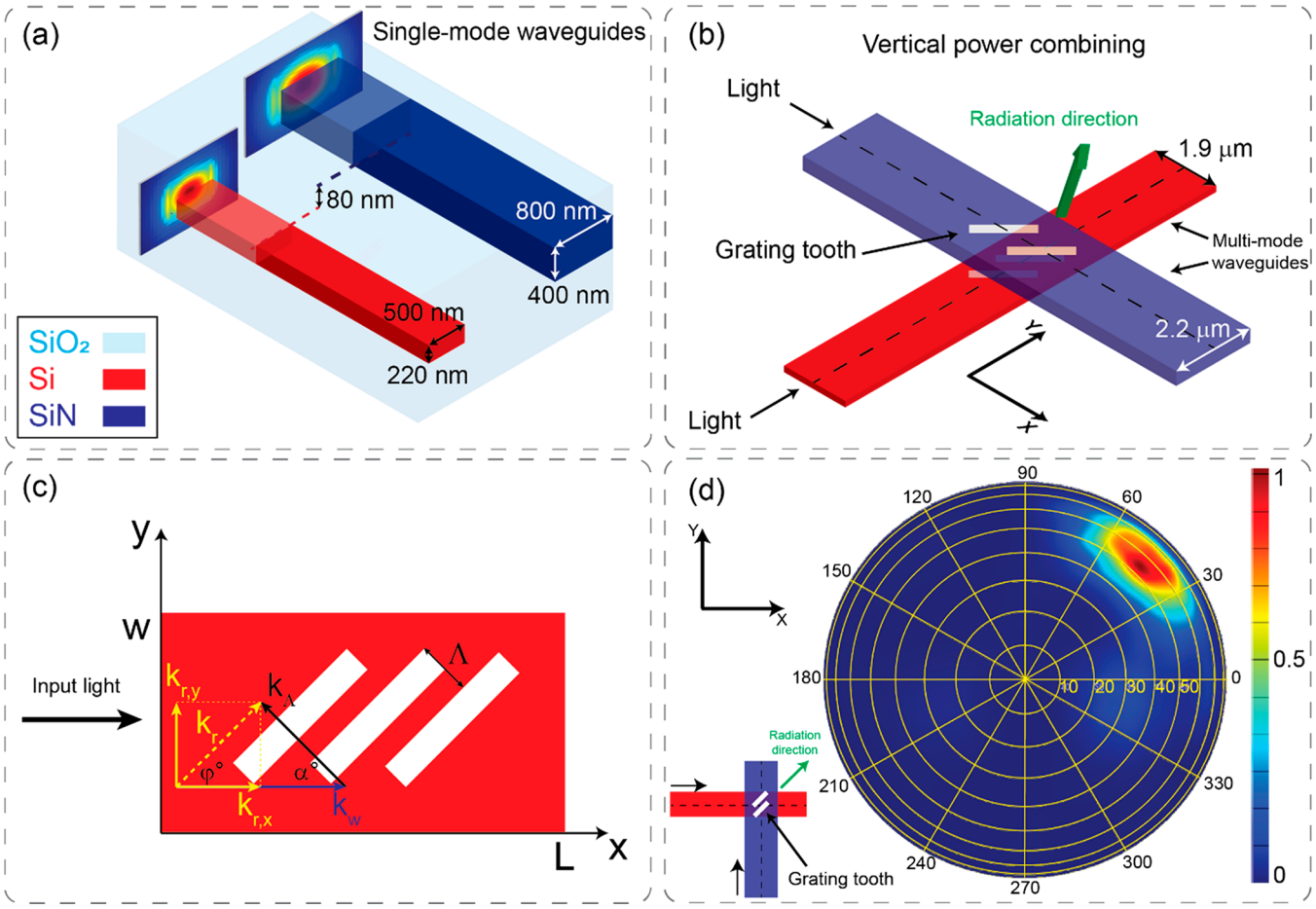

Figure 1. Tilted vertically stacked optical grating structures serving as nanoantennas. (a) Two single-mode waveguides in Si and SiN layers and the corresponding dimensions and optical mode profiles showing the photonic layer-stack of the fabrication process. The vertical distance between Si and SiN layers is 80 nm. Single-mode waveguides are used for on-chip optical routings. (b) Two vertically aligned tilted grating structures (nanoantennas) on multimode Si and SiN waveguides. Nanoantennas are 45° tilted with respect to the corresponding waveguide axis (dashed lines). (c) Structure of a multimode waveguide with tilted grating structures. (d) Simulated far-field interference pattern of tilted vertically aligned optical nanoantennas shown in Figure 1c in which an azimuth angle of about 45° with respect to each waveguide axis is observed.

optical routings are implemented using single-mode waveguides. The grating structures are implemented on multimode waveguides. Figure 1b shows vertically aligned tilted grating structures serving as nanoantennas implemented using two multimode waveguides on Si and SiN layers. The vertically stacked nanoantennas are tilted by 45° with respect to the central axis of the feed waveguides (dashed lines) in their respective layers (i.e., Si and SiN). As a result, the optical waves emitted from perpendicular Si and SiN waveguides (serving as nanoantenna feed lines) are aligned. Note that the green arrow in Figure 1b shows the direction of radiation. Also note that, for the structure in Figure 1b, the simulated undesired coupling between the Si and SiN layers is at least 20× lower than the desired signal within each waveguide and has a negligible effect on the far-field interference pattern and beam steering performance. Furthermore, simulations show that the reflected optical power due to the layer stacking is negligible. In addition, the tilted grating structures reduce the back-reflection.[22] Figure 1c shows tilted grating structures implemented on a waveguide as a nanoantenna with a length of L and a width of w, where k_w, k_r, k_Λ, Λ, and α are the wave vector of the optical wave in the waveguide, the wave vector of the radiated light projected on the $X-Y$ plane, the reciprocal lattice vector, the grating period, and the tilt angle of the grating structure with respect to the waveguide axis, respectively. At a given wavelength, for the tilted grating structure to radiate in the desired direction (specified by θ and φ, the zenith angle with respect to z axis, and the azimuth angle with respect to x axis, respectively), the grating tilt angle and the grating period must be set, which using the vector diagram in Figure 1c can be calculated as[22]

$$\tan \alpha = \frac{n_c \sin \theta \sin \varphi}{n_w - n_c \sin \theta \cos \varphi} \quad (1)$$

$$\Lambda = \frac{\lambda_0 \cos \alpha}{n_w - n_c \sin \theta \cos \varphi} \quad (2)$$

where n_w, n_c, and λ_0 are the effective index of refraction of the waveguide with gratings, the effective index of refraction of the medium around the waveguide (i.e., the cladding), and the wavelength of light in free space, respectively. In this case, the direction of radiation (the peak of the main lobe) is given by

https://doi.org/10.1021/acsphotonics.1c00608
ACS Photonics XXXX, XXX, XXX−XXX

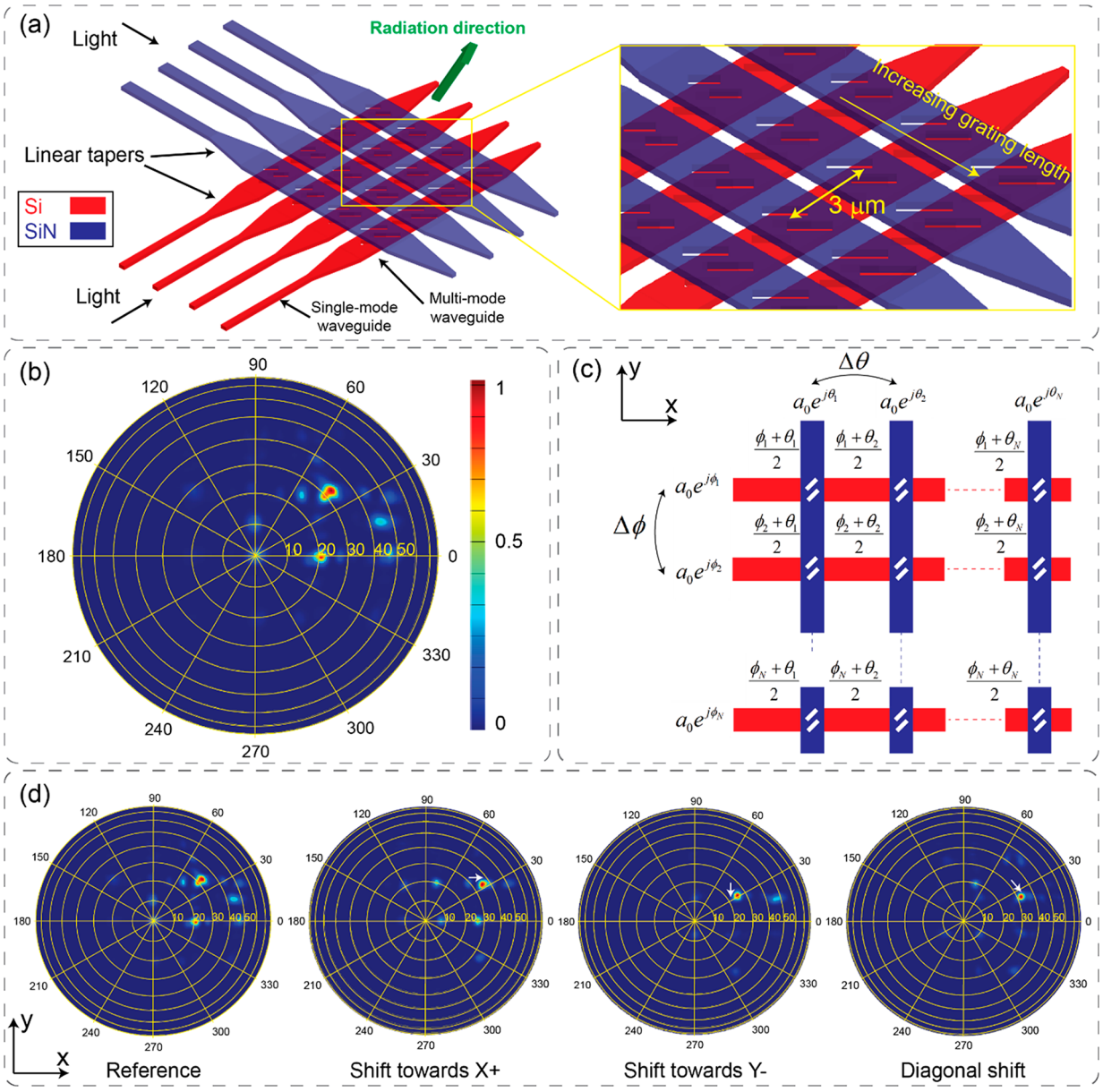

Figure 2. Simulated beam-steering performed using an OPA with vertically stacked nanoantennas. (a) The schematic of a 4 × 4 OPA formed using two vertically aligned 4 × 4 arrays on Si and SiN layers with element-spacing of 3 μm. The length of grating structures on each feed waveguide is gradually increased (in the direction of propagation) such that equal power is emitted from nanoantennas. (b) Simulated intensity of the far-field interference pattern of the OPA. (c) Conceptual schematic of an $N \times N$ OPA with $2N$ off-aperture phase shifters. The electric fields at the input of the m^{th} row waveguide and the n^{th} column waveguide have the same amplitude of a_0 and phases of ϕ_m and θ_n, respectively, resulting in a phase of $(\phi_m + \theta_n)/2$ for the element at the intersection of the two waveguides. To perform 2-D steering of a single optical beam, the relative phase between the adjacent nanoantennas in rows and columns can be set to $\Delta\phi_{m+1,m,n} = \Delta\phi$ and $\Delta\theta_{m,n+1,n} = \Delta\theta$, respectively. More details on off-aperture phase adjustment are presented in the Supporting Information S2. (d) Simulated 2-D beam-steering using the 4 × 4 OPA; steering toward $X+$ ($\Delta\phi$ = 120°, $\Delta\theta$ = 0°), $Y-$ ($\Delta\phi$ = 0°, $\Delta\theta$ = −120°), and diagonal ($\Delta\phi$ = 120°, $\Delta\theta$ = −120°).

$$\theta = \sin^{-1}\left(\frac{1}{n_c}\sqrt{\left(\frac{\lambda_0}{\Lambda}\right)^2 + n_w^2 - 2n_w\left(\frac{\lambda_0}{\Lambda}\right)\cos\alpha}\right)$$

$$\text{and} \quad \varphi = \tan^{-1}\left(\frac{\lambda_0 \sin\alpha}{n_w\Lambda - \lambda_0\cos\alpha}\right) \tag{3}$$

Equation 3 shows the dependency of the azimuth and zenith angles of radiation for a tilted grating structure on the grating and waveguide design parameters. Therefore, the waveguides and the vertically stacked grating structures in Si and SiN must be designed to ensure the same direction of propagation, that is, $\theta = \theta_{Si} = \theta_{SiN}$ and $\varphi = \varphi_{Si} = \varphi_{SiN}$, where $(\theta_{Si}, \varphi_{Si})$ and $(\theta_{SiN}, \varphi_{SiN})$ represent the direction of the optical beam radiated from the Si and SiN grating structures, respectively. Using eq 3, the beam alignment condition is written as

$$n_{w,Si}\Lambda_{Si} = n_{w,SiN}\Lambda_{SiN}$$

$$\text{and} \quad \frac{\lambda_0^2 + n_{w,Si}^2\Lambda_{Si}^2 - \sqrt{2}\lambda_0 n_{w,Si}\Lambda_{Si}}{\lambda_0^2 + n_{w,SiN}^2\Lambda_{SiN}^2 - \sqrt{2}\lambda_0 n_{w,SiN}\Lambda_{SiN}} = \frac{n_{c,Si}^2\Lambda_{Si}^2}{n_{c,SiN}^2\Lambda_{SiN}^2} \tag{4}$$

where $n_{w,Si}$, $n_{w,SiN}$, $n_{c,Si}$, $n_{c,SiN}$, Λ_{Si}, and Λ_{SiN} are the effective refractive index of Si and SiN waveguides (in the presence of

https://doi.org/10.1021/acsphotonics.1c00608
ACS Photonics XXXX, XXX, XXX−XXX

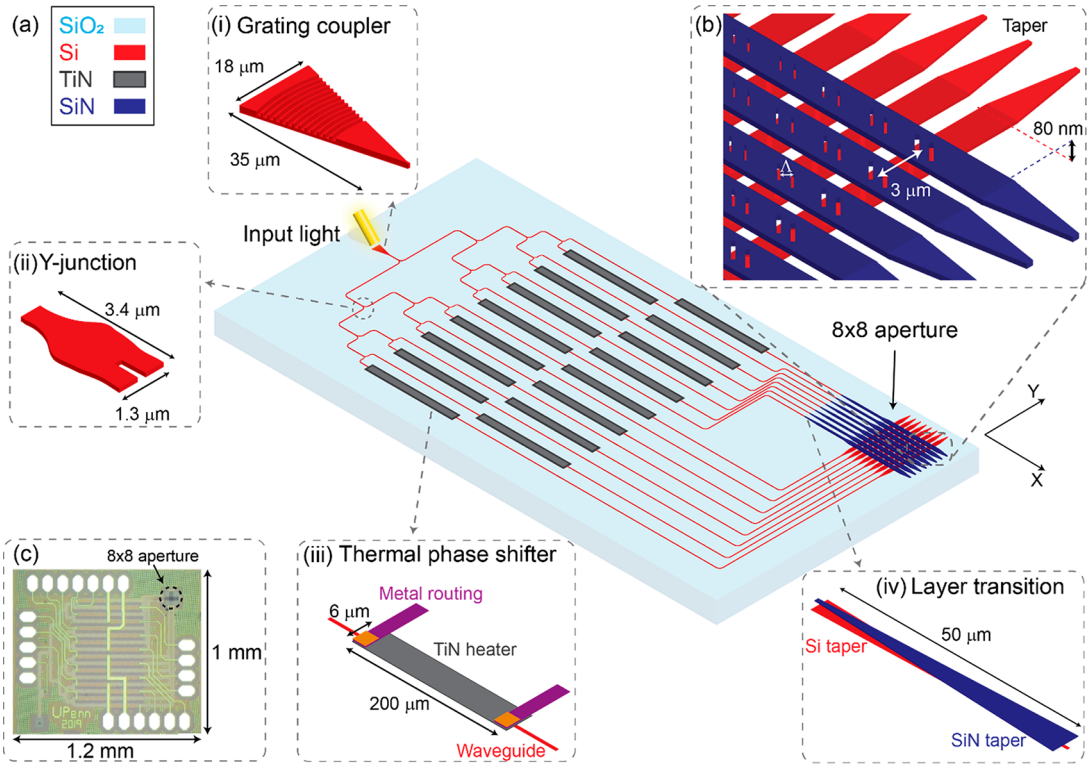

(d)

Single grating tooth	1	2	3	4	5	6	7	8
Si: Length/width (μm)	0.8/0.2	1/0.2	0.8/0.2	1.2/0.2	1.1/0.25	1.5/0.25	1.5/0.2	1.7/0.25
SiN: Length/width (μm)	0.7/0.2	1/0.2	1.2/0.2	1.3/0.2	1.5/0.2	1.8/0.2	1.8/0.35	2/0.55

* Dimensions are given for a single grating tooth of each nanoantenna.

Figure 3. Implemented 8 × 8 compact multilayer OPA. (a) The schematic of the proposed OPA implemented on Si and SiN device layers is shown. The input light is coupled into the chip using a grating coupler (i) and is split into 16 branches using Y-junctions (ii). The thermal phase shifter shown in (iii) consists of a TiN metal heater placed on top of a Si waveguide. The photonic layer transition (iv) consists of two vertically stacked Si and SiN waveguide tapers. (b) Zoomed-in view of the multilayer aperture of the OPA showing the nanoantennas in Si (with 110 nm partial-etch) and SiN (with 400 nm full etch) vertically stacked with 80 nm spacing to combine the row and column signals in the near-field. (c) The microphotograph of the OPA chip implemented in the Tower Semiconductor 180 nm silicon photonic process. (d) The width and length of the individual teeth of the grating structures serving as nanoantennas of the 8 × 8 OPA implemented in Si and SiN layers.

grating structures and srounding structures), the effective refractive index of the cladding of Si and SiN grating structures, and the grating period for Si and SiN gratings, respectively, and $\alpha = 45°$ is assumed. Note that in the fabrication process used in this work, the close proximity of Si and SiN affects the effective index of refraction of each waveguide with grating structures as well as that of the cladding surrounding each waveguide, making the estimation of these effective refractive indices more complex compared to a conventional grating coupler, where only one material (Si or SiN) is used. Therefore, electromagnetic simulations were used to fine-tune the design of the vertically stacked nanoantennas to ensure that the beams emitted by the two layers are aligned. The simulated far-field pattern of the stacked nanoantennas in Figure 1b is shown in Figure 1d, where an azimuth angle of radiation of about 45° (with respect to the central axis of feed waveguides) is observed. Note that, for the tilt angle of 45°, the azimuth angle of radiation can be adjusted by setting the waveguide dimensions, grating periods, and the wavelength of operation. The calculation of the far-field radiation pattern of the tilted grating structure nanoantennas is presented in the Supporting Information, S3.

Figure 2a shows an array of vertically stacked tilted nanoantennas formed in Si and SiN layers, which is used to simulate beam forming. Within the near-field of two vertically stacked nanoantennas, the light emitted from the tilted nanoantenna implemented on the bottom Si waveguide is vertically combined with the light emitted from the corresponding tilted nanoantenna implemented on the top SiN layer. To reduce the nanoantenna pitch, tilted nanoantennas are implemented on multimode feed waveguides for both bottom and top layers. To ensure equal emitted power from nanoantennas on each feed waveguide, the length of the grating structures is gradually increased while the grating period is kept constant (Figure 2a).

Note that if the aspect ratio of a grating tooth approaches unity (corresponding to a square grating tooth), the far-field pattern of a resulting nanoantenna would be symmetric ($\varphi \approx 0°$), since a symmetric scatterer with respect to the waveguide axis radiates symmetrically with respect the same axis. This sets the minimum achievable length of the first nanoantenna on the feed waveguide given the grating period. Therefore, in designing the grating structures of nanoantennas, the aspect ratios are carefully chosen. Linear tapered waveguides are used

https://doi.org/10.1021/acsphotonics.1c00608
ACS Photonics XXXX, XXX, XXX−XXX

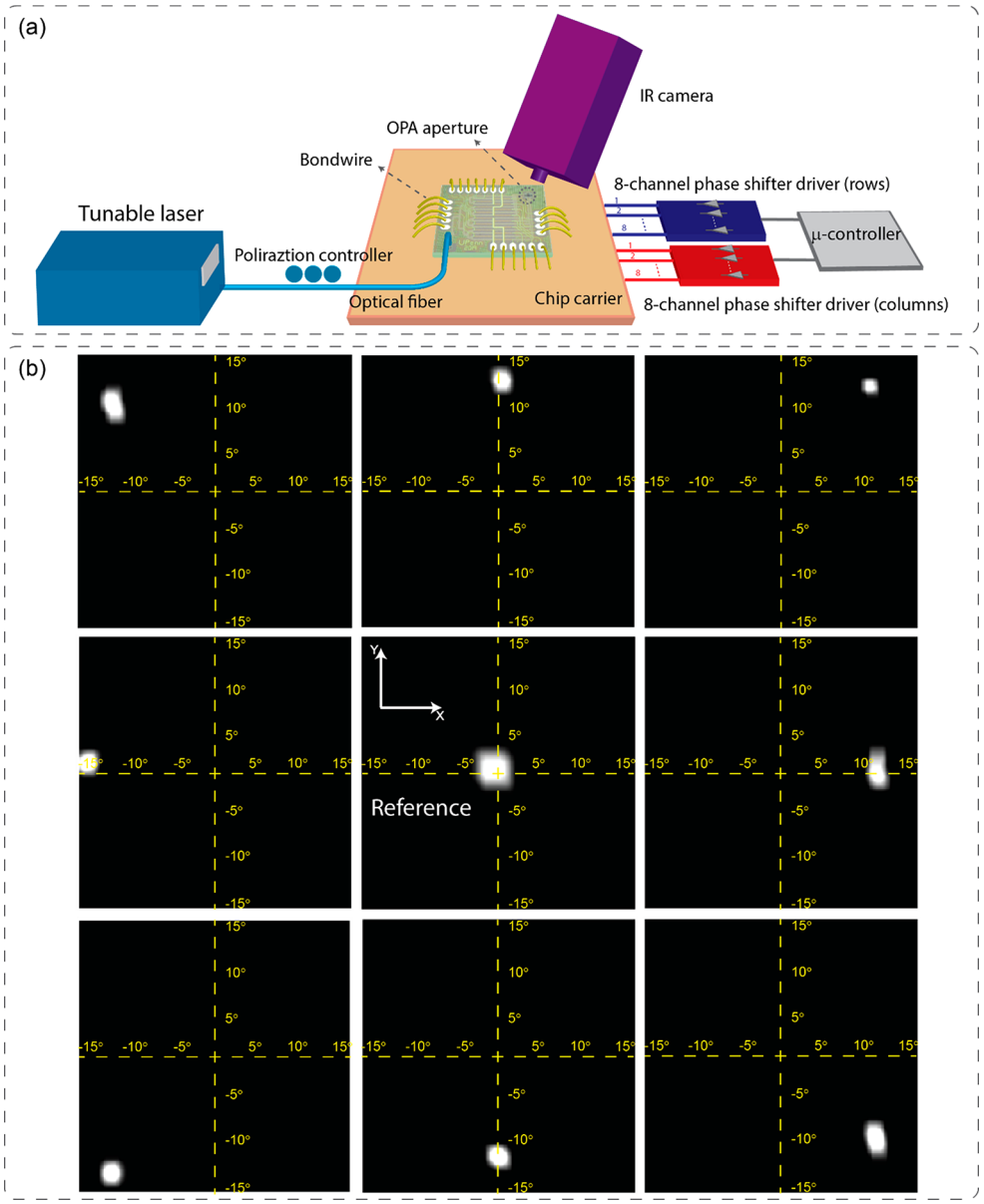

Figure 4. 2-D beam-steering demonstration. (a) The measurement setup. The −3 dBm input light at 1470 nm is coupled into the chip using an optical fiber after polarization adjustment. Two 8-channel phase shifter drivers, with 8-bit per channel resolution are used. A microcontroller sets the digital control signals of the drivers. The far-field interference pattern is monitored using a FJW FIND-R-Scope 85700A IR camera. (b) 2-D beam-steering demonstration using the implemented multilayer OPA chip. A beam-steering range of about 23° is achieved.

as a transition between single-mode routing waveguides and multimode feed waveguides. To verify the beam-forming performance of the proposed OPA architecture, the far-field pattern of a 4 × 4 OPA with vertically stacked tilted nanoantennas is simulated, which is shown in Figure 2b.

In order to reduce the photonic routing complexity allowing for more closely placed OPA elements, off-aperture phase adjustment was utilized. For an $N \times N$ OPA, N phase shifters can be used outside the OPA aperture to set the relative phase between N rows of Si feed waveguides. Similarly N off-aperture phase shifters can be used to set the relative phase between N columns of SiN feed waveguides. In such a remote phase adjustment method,[21] as shown in Figure 2c, the required relative phase between the elements for 2-D beam-steering can be set by adjusting the phase of the optical waves in row and column waveguides. This approach significantly reduces the photonic and electrical routing complexities as well as the system power consumption and the metallic-induced optical loss within the aperture. This method is explained in more details in the Supporting Information S2. Figure 2d shows the simulated beam-steering for the array of 4 × 4 vertically stacked tilted nanoantennas shown in Figure 2a.

Figure 3a shows the structure of the implemented 8 × 8 multilayer OPA chip with two vertically stacked device layers of Si and SiN with 80 nm vertical spacing. Since, for the same SiO_2 cladding, Si offers a higher optical confinement due to a larger refractive index compared to SiN, it is the preferred layer for implementation of the optical routing due to a higher degree of integration, which results in a smaller chip area.

The input light is coupled into the chip using a grating coupler implemented in the Si layer and is split into 16 branches using 4 layers of Y-junctions, resulting in 8 row

https://doi.org/10.1021/acsphotonics.1c00608
ACS Photonics XXXX, XXX, XXX−XXX

signals and 8 column signals. Within each row/column waveguide, the phase of the optical wave is adjusted using a thermal phase shifter. The phase-adjusted signals are routed to two vertically stacked 8 × 8 arrays of nanoantennas: one in Si (red, rows) and one in SiN (blue, columns), as shown in Figure 3a. The transition of light between Si waveguides and SiN waveguides takes place through vertical evanescent coupling. Tilted vertically stacked nanoantennas with a 3 μm pitch are implemented through partially and fully etching the Si and SiN multimode waveguides, respectively. Note that, given the effective refractive indices of Si and SiN and the wavelength of operation, the grating structures are designed and placed at 45° with respect to the axis of the feed waveguides to align and vertically combine optical waves emitted from the stacked nanoantennas. The microphotograph of the OPA chip implemented in the Tower Semiconductor 180 nm silicon-on-insulator photonic process is shown in Figure 3c. Figure 3d shows the dimensions of the individual grating teeth forming the nanoantennas that are designed to ensure the same per-element radiated power. The grating periods (Λ in Figure 3b) on Si and SiN layers are 500 and 840 nm, respectively. The characterization of Si and SiN nanoantennas is discussed in Supporting Information S1. An array of digitally controlled phase shifter drivers are used to control the relative phase between rows of Si feed waveguides. Similarly, the relative phase between columns of SiN feed waveguides is adjusted. The far-field interference pattern of the multilayer OPA is monitored using an infrared camera.

Prior to the beam-steering demonstration, the OPA chip was calibrated in two steps: first, the array-level beam alignment at the wavelength of interest was performed, where the effect of the difference between the relative phases of the adjacent nanoantennas on the Si and SiN feed waveguides (due to the refractive index difference between Si and SiN layers) is compensated by adding a constant phase offset between the SiN (column) waveguides (see Supporting Information S4 for more details). After OPA output beam alignment, a previously reported procedure[21] was utilized to perform a phase calibration to account for the phase mismatch between array elements caused by process variations.

After calibration, 2-D beam-steering was demonstrated (Figure 4b). Given the image sensor size of the IR camera and the distance between the image sensor of the camera and the OPA aperture, Figure 4b suggests a beam-steering range of about 23°. Note that given the structure of the implemented OPA and the wavelength of operation, a theoretical steering range of about 28° is calculated.

The total optical loss from the input grating coupler to each nanoantenna on Si and SiN layers is about 48 dB (see Supporting Information S5 for more details). In this case, given 128 nanoantennas (64 on each layer), for a −3 dBm input optical power, the power in the main radiation lobe is estimated to be about −30 dBm.

Note that the low emitted power from each grating structure is due to its small size. Therefore, for the same input optical power, the optical power within the main lobe can be significantly increased if more grating structures are placed on each waveguide, utilizing a rather large unused optical power (instead of scattering it though tapers at the end of row and column waveguides in the implemented prototype).

Note that due to the limited dynamic range and nonlinear response of the IR camera, and to avoid saturation of the detected main lobe, the input optical power to the OPA needs to be reduced. As a result, and due to the limited sensitivity of the IR camera, the measured power of the side lobes and the background appear to be considerably lower than those in the simulated far-field (e.g., in Figure 2d).

In conclusion, we present and demonstrate a novel multilayer single-wavelength OPA for 2-D beam steering that benefits from 3-D light distribution and processing with off-aperture phase adjustment enabling compact element-spacing. The proposed vertically stacked grating structures forming the OPA nanoantennas eliminate the need for devices such as directional couplers or Y-junctions that are conventionally used for optical power combining and distribution. As a proof of concept, a compact 8 × 8 OPA with a record element pitch of 3 μm and only 16 off-aperture phase shifters is implemented using a commercially available silicon photonic process with two photonic device layers (i.e., Si and SiN). Furthermore, 2-D optical beam steering over a range of about 23° is demonstrated using the implemented OPA chip.

■ ASSOCIATED CONTENT

Supporting Information

The Supporting Information is available free of charge at https://pubs.acs.org/doi/10.1021/acsphotonics.1c00608.

Nanoantenna characterization; $N \times N$ OPA with $2N$ off-aperture phase control theory of operation; tilted grating nanoantenna radiation pattern calculation; OPA output beam alignment calibration; photonic chip fabrication and optical path loss; measurement devices and equipment; Figures S1−S4, and Table S1 (PDF)

■ AUTHOR INFORMATION

Corresponding Author

Farshid Ashtiani − *Department of Electrical and Systems Engineering, University of Pennsylvania, Philadelphia, Pennsylvania 19104, United States;* orcid.org/0000-0002-8418-9626; Email: farshid@seas.upenn.edu

Author

Firooz Aflatouni − *Department of Electrical and Systems Engineering, University of Pennsylvania, Philadelphia, Pennsylvania 19104, United States*

Complete contact information is available at: https://pubs.acs.org/10.1021/acsphotonics.1c00608

Author Contributions

The manuscript was written through contributions of all authors. All authors have given approval to the final version of the manuscript.

Notes

The authors declare no competing financial interest.

■ ACKNOWLEDGMENTS

This work was partially funded under Defense Advanced Research Projects Agency MOABB Program (FA8650-18-1-7828) and partially under National Aeronautics and Space Administration ESI Program (80NSSC19K0214).

■ REFERENCES

(1) Xie, W.; Komljenovic, T.; Huang, J.; Tran, M.; Davenport, M.; Torres, A.; Pintus, P.; Bowers, J. Heterogeneous silicon photonics sensing for autonomous cars [Invited]. *Opt. Express* **2019**, *27*, 3642−3663.

(2) Sun, J.; Timurdogan, E.; Yaacobi, A.; Shah Hosseini, E.; Watts, M. R. Large-scale nanophotonic phased array. *Nature* **2013**, *493*, 195−199.
(3) Poulton, C. V.; Byrd, M. J.; Russo, P.; Timurdogan, E.; Khandaker, M.; Vermeulen, D.; Watts, M. R. Long-Range LiDAR and Free-Space Data Communication With High-Performance Optical Phased Arrays. *IEEE J. Sel. Top. Quantum Electron.* **2019**, *25*, 1−8.
(4) Aflatouni, F.; Abiri, B.; Rekhi, A.; Hajimiri, A. Nanophotonic projection system. *Opt. Express* **2015**, *23*, 21012−21022.
(5) Aflatouni, F.; Abiri, B.; Rekhi, A.; Hajimiri, A. Nanophotonic coherent imager. *Opt. Express* **2015**, *23*, 5117−5125.
(6) Spector, S. J.; Lane, B. F.; Watts, M. R.; Benney, L. D.; Delva, J. G.; Hare, A. E.; Kelsey, A. F.; Mlynarczyk, J. M.; Hosseini, E. S.; Poulton, C. V.; Laine, J. P. Broadband Imaging and Wireless Communication with an Optical Phased Array. *Conference on Lasers and Electro-Optics, OSA Technical Digest (online)*; Optical Society of America, 2018, paper SM3I.7, DOI: 10.1364/CLEO_SI.2018.SM3I.7.
(7) Abediasl, H.; Hashemi, H. Monolithic optical phased-array transceiver in a standard SOI CMOS process. *Opt. Express* **2015**, *23*, 6509−6519.
(8) Chung, S.; Abediasl, H.; Hashemi, H. A 1024-element scalable optical phased array in 0.18 μm SOI CMOS. *IEEE International Solid-State Circuits Conference (ISSCC)*; IEEE, 2017, DOI: 10.1109/ISSCC.2017.7870361.
(9) Poulton, C. V.; Russo, P.; Timurdogan, E.; Whitson, M.; Byrd, M. J.; Hosseini, E.; Moss, B.; Su, Z.; Vermeulen, D.; Watts, M. R. High-Performance Integrated Optical Phased Arrays for Chip-Scale Beam Steering and LiDAR. *Conference on Lasers and Electro-Optics, OSA Technical Digest (online)*; Optical Society of America, 2018, paper ATu3R.2, DOI: 10.1364/CLEO_AT.2018.ATu3R.2.
(10) Fatemi, R.; Khachaturian, A.; Hajimiri, A. A Nonuniform Sparse 2-D Large-FOV Optical Phased Array With a Low-Power PWM Drive. *IEEE J. Solid-State Circuits* **2019**, *54*, 1200−1215.
(11) Zhang, L.; Li, Y.; Tao, M.; Wang, Y.; Hou, Y.; Chen, B.; Li, Y.; Qin, L.; Gao, F.; Luo, X.; Lo, G.; Song, J. Large-scale integrated multi-lines optical phased array chip. *IEEE Photonics J.* **2020**, *12*, 1−8.
(12) Doylend, J. K.; Heck, M. J. R.; Bovington, J. T.; Peters, J. D.; Coldren, L. A.; Bowers, J. E. Two-dimensional free-space beam steering with an optical phased array on silicon-on-insulator. *Opt. Express* **2011**, *19*, 21595−21604.
(13) Hutchison, D. N.; Sun, J.; Doylend, J. K.; Kumar, R.; Heck, J.; Kim, W.; Phare, C. T.; Feshali, A.; Rong, H. High-resolution aliasing-free optical beam steering. *Optica* **2016**, *3*, 887−890.
(14) Hulme, J. C.; Doylend, J. K.; Heck, M. J. R.; Peters, J. D.; Davenport, M. L.; Bovington, J. T.; Coldren, L. A.; Bowers, J. E. Fully integrated hybrid silicon two dimensional beam scanner. *Opt. Express* **2015**, *23*, 5861−5874.
(15) Komljenovic, T.; Helkey, R.; Coldren, L.; Bowers, J. E. Sparse aperiodic arrays for optical beam forming and LIDAR. *Opt. Express* **2017**, *25*, 2511−2528.
(16) Van Acoleyen, K.; Rogier, H.; Baets, R. Two-dimensional optical phased array antenna on silicon-on-insulator. *Opt. Express* **2010**, *18*, 13655−13660.
(17) Miller, S. A.; Chang, Y.; Phare, C. T.; Shin, M. C.; Zadka, M.; Roberts, S. P.; Stern, B.; Ji, X.; Mohanty, A.; Gordillo, O. A. J.; Dave, U. D.; Lipson, M. Large-scale optical phased array using a low-power multi-pass silicon photonic platform. *Optica* **2020**, *7*, 3−6.
(18) Poulton, C. V.; Byrd, M. J.; Moss, B.; Timurdogan, E.; Millman, R.; Watts, M. R.; 8192-Element Optical Phased Array with 100° Steering Range and Flip-Chip CMOS. *Conference on Lasers and Electro-Optics, OSA Technical Digest*; Optical Society of America, 2020, paper JTh4A.3, DOI: 10.1364/CLEO_AT.2020.JTh4A.3.
(19) Phare, C. T.; Shin, M. C.; Sharma, J.; Ahasan, S.; Krishnaswamy, H.; Lipson, M. Silicon Optical Phased Array with Grating Lobe-Free Beam Formation Over 180 Degree Field of View. *Conference on Lasers and Electro-Optics, OSA Technical Digest (online)*; Optical Society of America, 2018, paper SM3I.2, DOI: 10.1364/CLEO_SI.2018.SM3I.2.
(20) Kong, Z.; Lee, Y. J.; Noman, A. A.; Tang, Y.; Chang, G.; Chen, R.; Qi, M. Aliasing-free Beam Steering from an Optical Array Emitter with Half-wavelength Pitch. In *OSA Advanced Photonics Congress (AP) 2020*; Caspani, L., Tauke-Pedretti, A., Leo, F., Yang, B., Eds.; OSA Technical Digest, Optical Society of America, 2020, paper ITh2H.6, DOI: 10.1364/IPRSN.2020.ITh2H.6.
(21) Ashtiani, F.; Aflatouni, F. N × N optical phased array with 2N phase shifters. *Opt. Express* **2019**, *27*, 27183−27190.
(22) Li, Y.; Li, L.; Tian, B.; Roelkens, G.; Baets, R. G. Reflectionless Tilted Grating Couplers With Improved Coupling Efficiency Based on a Silicon Overlay. *IEEE Photonics Technol. Lett.* **2013**, *25*, 1195−1198.

https://doi.org/10.1021/acsphotonics.1c00608
ACS Photonics XXXX, XXX, XXX−XXX